Hindawi
Mathematical Problems in Engineering
Volume 2018, Article ID 5942890, 12 pages
https://doi.org/10.1155/2018/5942890

Research Article

Detection of Broken Rotor Bars Fault in Induction Motors by Using an Improved MUSIC and Least-Squares Amplitude Estimation

Junjie Lu, Panpan Wang, Sen Duan, Liping Shi, and Li Han

School of Electrical and Power Engineering, China University of Mining and Technology, Xuzhou 221116, China

Correspondence should be addressed to Panpan Wang; wangpanpan@cumt.edu.cn

Received 15 September 2018; Accepted 31 October 2018; Published 15 November 2018

Academic Editor: Isabel S. Jesus

The frequencies and amplitudes of the broken rotor bar (BRB) fault features are the basis for the accurate diagnosis of the BRB fault. However, how to accurately detect their frequency and amplitudes has always been a difficult problem for induction motor fault detection. For this problem, a new fault detection method based on an improved multiple signal classification (MUSIC) and least-squares magnitude estimation is proposed. First, since the fixed-step traversal search reduces the computational efficiency of MUSIC, a niche bare-bones particle swarm optimization (NBPSO) for multimodal peaks search is proposed to improve MUSIC, which is used to compute the frequency values of fault-related and fundamental components in stator current signal. Second, using these frequency values, a fault current signal model is established to convert the magnitude estimation problem into a linear least-squares problem. On this basis, the amplitudes and phases of fault-related and fundamental components could be estimated accurately with the singular value decomposition (SVD). A simulation signal is used to test the new method and the results show that the proposed method not only has higher frequency resolution, but also improves estimation accuracy of parameters greatly even with short data window. Finally, experiments for a real induction motor are performed, and the effectiveness and superiority of the proposed method are proved again.

1. Introduction

Induction motors have been widely applied in the fields of industry and agriculture because of its simple structure, long life, low cost, and so on. In fact, most motors operate in a poor working environment, such as overloading, frequently starting and braking. Meanwhile, due to the too much mechanical and thermal stress, as well as some inherent defects of the rotor, the appearance of BRB or end ring cracking is a common phenomenon. During early stage, such as one broken bar, this type of fault may not show any symptoms. If no detection system or program, such fault will gradually deteriorate, causing other faults or leading to the sudden collapse [1–3]. It is known that unplanned downtime often causes a great economic loss [3]. So BRB fault detection for induction motor is necessary in early stage.

When BRB failure occurs, additional current components, whose frequency are $f_{brk}=(1\pm 2ks)f_1$, will appear in the stator current. Here, f_1 is the power frequency, s is the slip, and k is a positive integer. These current components are viewed as the features of BRB fault. Since the stator current signal is collected easily, its spectrum analyzed by the discrete Fourier transform (DFT) is widely used to detect BRB fault. However, when the motor is in the steady state, the small slip makes the frequencies of the strongest fault-related components very close to the fundamental frequency. Meanwhile, they are relatively weak and easy to be submerged by the leakage of fundamental harmonic or noise. The above two points expect signal processing methods to have functions of high frequency resolution and elimination of the fundamental leakage. For the influence of fundamental harmonic, many distinctive detection methods based on DFT are proposed to eliminate its influence [4–9]. The main idea of these methods is to filter the fundamental harmonic directly or convert it into DC component, and then the DFT is used to analyze the preprocessed current signal. In other

papers, filtered Park's vector modulus [10], product of current and virtual flux [11] and instantaneous power [12] analyzed through DFT have been used in BRB detection. Although these methods improve the reliability of the BRB detection, they cannot avoid the inherent shortcoming of DFT. For instance, the frequency resolution is inversely proportional to the sampling time. This means that, it requires a long enough sampling time and large memory space to get a high frequency resolution. However, in real application, long sampling time will cause the increase of the probability of disturbances, affecting the reliability of fault detection [13]. To reduce the memory space and compute cost, a sub-Nyquist strategy with reduced data length [14] and a diagnostic signal designated as the reduced envelope of the stator current [15] are introduced into detection methods. At the same time, harmonic order tracking analysis [15, 16] and side-lobes leakage phenomenon of the sliding DFT [17] are used in BRB detection to lessen the dependence on frequency resolution. Another problem of DFT-based methods is the amplitude estimation of the fault-related components which is used to calculate the fault severity. Due to spectrum leakage and fence effect, DFT has no ability to estimate them accurately with short-time data window [13].

MUSIC is one of the modern spectral estimation methods known as subspace techniques. Due to the original signal extrapolation ability, its frequency resolution can get rid of the limitation of the data window. Therefore, MUSIC algorithm also was applied in the analysis of stator current [18], radial flux signal [19], and zero-sequence current [20] for BRB detection. To eliminate the influence of the fundamental harmonic, the eigenvector corresponding to fundamental harmonic in signal subspace was moved to the noise subspace to construct a new noise subspace [21]. This improved algorithm cannot only eliminate the influence of fundamental harmonic, but also improve the frequency resolution. Combining other techniques, such as spectrum zooming technique [22] and empirical mode decomposition [23], is another way to improve detection performance of the MUSIC. Although MUSIC has been applied successfully in the detection of BRB fault, it still has two shortcomings: (1) due to the fixed-step traversal search, it is not efficient for the spectrum peak search; (2) MUSIC cannot determine the other parameter values of each component, such as initial phase and amplitude. To solve the 2th-problem, an improved MUSIC algorithm which combines MUSIC with the pattern search algorithm is proposed [24]. However, this method needs a good starting point by DFT, and a long computational time.

In this paper, MUSIC, particle swarm intelligence search and least-square technology are conjugated to improve estimate accuracy of the parameters of fault-related and fundamental components for BRB fault detection. For the shortages of MUSIC, we modify MUSIC from two aspects. To improve the efficiency of the spectrum peak search, a niche bare-bones particle swarm optimization (NBPSO) is proposed, replacing the fixed-step traversal search; on the other hand, the least-squares criterion is used to estimate the magnitude and phase of each component in the stator current. In simulation test, the DFT and traditional MUSIC are also selected for comparison. Finally, the proposed method combining the improved MUSIC with least-squares magnitude estimation is applied to the BRB fault detection for a real induction motor.

2. Related Concepts and Methods

2.1. Multiple Signal Classification. Multiple signal classification (MUSIC) was raised by Schmidt R. O. in 1986 [25]. It is a subspace method that can detect the frequencies of complex sinusoids using matrix eigenvalue decomposition. Its main idea is described as follows. First, the information space of observation signal is divided into two orthogonal subspaces by eigenvalue decomposition, i.e., the signal subspace and noise subspace; second, the spectrum is structured with the orthogonality of two subspaces to estimate the frequency of each component in the signal. MUSIC assumes that the discrete-time signal can be represented as a data model, that is

$$y(n) = \sum_{i=1}^{P/2} A_i \cos\left(2\pi F_i n + \varphi_i\right) + h(n), \tag{1}$$

where $n = 1, 2, 3, \ldots$; P/2 is the number of pure sinusoids; A_i, F_i, φ_i are the amplitude, frequency, and initial phase of the *i-th* pure sinusoids, respectively; *h(n)* is the complex white noise with a zero mean and a variance τ^2.

According to Euler's formula, $y(n)$ can also be expressed as

$$y(n) = \sum_{i=1}^{P} a_i e^{j(2\pi f_i n + \varphi_i)} + h(n), \tag{2}$$

where $a_i = A_i/2$, $f_i = F_i$, $f_{P/2+i} = -F_i$, for $1 \le i \le P/2$.

For M serial observed signal, (2) is constructed as

$$\begin{aligned} \boldsymbol{Y}(n) &= \left[y(n) \quad y(n+1) \quad \cdots \quad y(n+M-1)\right] \\ &= \sum_{i=1}^{P} \boldsymbol{s}_i(n) + h(n), \end{aligned} \tag{3}$$

where $M >> P$, $\boldsymbol{s}_i(n) = [1, e^{j2\pi f_i}, e^{j4\pi f_i}, \ldots, e^{j2\pi(M-1)f_i}]a_i e^{j2\pi f_i n}$.

If set $\boldsymbol{D}(f_i) = [1, e^{j2\pi f_i}, e^{j4\pi f_i}, \ldots, e^{j2\pi(M-1)f_i}]^T$, $\boldsymbol{FD} = [\boldsymbol{D}(f_1), \boldsymbol{D}(f_2), \ldots, \boldsymbol{D}(f_M)]$, $\boldsymbol{A} = [a_1 e^{j2\pi f_1 n}, a_2 e^{j2\pi f_2 n}, \ldots, a_M e^{j2\pi f_M n}]$, $\boldsymbol{Y}(n)$ is rewrote as

$$\boldsymbol{Y}(n) = \boldsymbol{FD} \cdot \boldsymbol{A} + h(n). \tag{4}$$

Here, $\boldsymbol{FD}$ is a $M \times P$ Vander monde matrix and also a space spanned by $\boldsymbol{D}(f_i)$.

The autocorrelation matrix of $\boldsymbol{Y}(n)$ is

$$\boldsymbol{R}_{yy} = E\left\{\boldsymbol{Y}(n)\boldsymbol{Y}^T(n)\right\} = \boldsymbol{FD} \cdot E\left\{\boldsymbol{A}\boldsymbol{A}^T\right\} \cdot \boldsymbol{FD}^T + \tau^2 \boldsymbol{I}, \tag{5}$$

where T represents the matrix conjugate transpose, E is the mathematical expectation, and $\boldsymbol{I}$ is an identity matrix.

The eigenvalue $\boldsymbol{\Sigma} = \{\lambda_1 \ge \lambda_2 \ge \ldots \ge \lambda_P \ge \lambda_{P+1} \ge \ldots \ge \lambda_M\}$ and corresponding eigenvector $\boldsymbol{U}_{SN} = \{\boldsymbol{U}_1, \boldsymbol{U}_2, \ldots, \boldsymbol{U}_M\}$ are derived from eigenvalue decomposition of the $\boldsymbol{R}_{yy}$. That is

$$\boldsymbol{R}_{yy} = \boldsymbol{U}_{SN}\boldsymbol{\Sigma}\boldsymbol{U}_{SN}^{T} = \begin{bmatrix}\boldsymbol{U}_S & \boldsymbol{U}_N\end{bmatrix}\begin{bmatrix}\boldsymbol{\Sigma}_S & 0\\ 0 & \boldsymbol{\Sigma}_N\end{bmatrix}\begin{bmatrix}\boldsymbol{U}_S & \boldsymbol{U}_N\end{bmatrix}^{T} = \boldsymbol{U}_S\boldsymbol{\Sigma}_S\boldsymbol{U}_S^{T} + \boldsymbol{U}_N\boldsymbol{\Sigma}_N\boldsymbol{U}_N^{T}. \quad (6)$$

In the space $\boldsymbol{U}_{SN}$, the subspace $\boldsymbol{U}_S$, as well as the space $\boldsymbol{FD}$, spanned by eigenvectors $\{\boldsymbol{U}_1, \boldsymbol{U}_2, \ldots, \boldsymbol{U}_P\}$ corresponding to Top-P larger eigenvalues is the signal subspace. The subspace $\boldsymbol{U}_N$ spanned by eigenvectors $\{\boldsymbol{U}_{P+1}, \boldsymbol{U}_{P+2}, \ldots, \boldsymbol{U}_M\}$ corresponding to the remaining eigenvalues is the noise subspace.

Since $\boldsymbol{U}_S$ and $\boldsymbol{U}_N$ are orthogonal, the vector of each signal component is also orthogonal to noise subspace, which is

$$\boldsymbol{D}(f_i) \perp \boldsymbol{U}_N. \quad (7)$$

According to (7), the MUSIC pseudospectrum is defined as

$$\mathrm{PM}(f) = \frac{1}{\left|\boldsymbol{D}(f)^{T} \cdot \boldsymbol{U}_N\right|^2}. \quad (8)$$

For one pure sinusoid component included in signal $y(n)$, if its frequency is f_i, PM(f) will have a peak at f_i. Therefore, the signal frequency estimation can be achieved by searching the peaks of PM (f) with the step Δf. In a real application, the $\boldsymbol{R}_{yy}$ need to be estimated using observation data.

The specific steps of traditional MUSIC are described as follows:

Step 1. Take a group of observation data and estimate the autocorrelation matrix $\boldsymbol{R}_{yy}$.

Step 2. Perform the eigenvalue decomposition of $\boldsymbol{R}_{yy}$ to generate the signal subspace $\boldsymbol{U}_S$ and the noise subspace $\boldsymbol{U}_N$.

Step 3. According to (8), calculate MUSIC pseudospectrum with the step Δf.

Step 4. Find all the peaks in the pseudospectrum, and then determine the frequencies of all pure sinusoids.

2.2. Particle Swarm Optimization. Particle swarm optimization (PSO) is a global optimization technique simulating behavior of biological colony [26]. For PSO, each particle represents a solution and has three intrinsic properties. Two of them are the position and velocity, respectively, represented by the vectors $\boldsymbol{x_i} = (x_{i1}, x_{i2}, \ldots, x_{iD})$ and $\boldsymbol{v_i} = (v_{i1}, v_{i2}, \ldots, v_{iD})$. The third is the fitness that is determined by the fitness function. Each particle keeps flying in feasible space and adjusts its flight path according to two extremum particles. One is its personal best position $\boldsymbol{p}_i$, i.e., its own flying experiences. The other is the global best position $\boldsymbol{p}_g$, i.e., its companions' flying experiences. PSO is an optimization tool based on iteration. For the $(t+1)$-th iteration, the position and velocity of each particle are updated by the following equations:

$$v_{i,j}(t+1) = wv_{i,j}(t) + c_1 r_1\left(p_{i,j}(t) - x_{i,j}(t)\right) + c_2 r_2\left(p_{g,j}(t) - x_{i,j}(t)\right) \quad (9)$$

$$x_{i,j}(t+1) = x_{i,j}(t) + v_{i,j}(t+1), \quad (10)$$

where w is an inertia weight, c_1, c_2 are two learning factors, r_1, r_2 are two random numbers in $[0,1]$, $v_{ij} \epsilon [-v_{\max}, v_{\max}]$, $v_{\max}$ is maximum velocity set by users, $i = 1, 2, \ldots, \mathrm{K}$, K is the number of the particle swarm, $j = 1, 2, \ldots, \mathrm{D}$, D is the dimension of the search space.

To simplify PSO, a bare-bones PSO algorithm (BBPSO) was proposed in 2003 [27]. In BBPSO, a Gaussian distribution about the position information of p_i and p_g is used to update the positions of all particles.

$$x_{i,j}(t+1) = N\left(\mu_{i,j}(t), \sigma_{i,j}^2(t)\right) \quad (11)$$

where $\mu_{i,j}(\mathrm{n}) = (p_{i,j}(n) + p_{g,j}(n))/2$ is the mean of the Gaussian distribution and $\sigma_{2i,j}(\mathrm{n}) = |p_{i,j}(\mathrm{n}) - p_{g,j}(\mathrm{n})|$ is the standard deviation of the Gaussian distribution. Compared with the standard PSO algorithm, BBPSO need not to set up control parameters, such as inertia weight and learning factor. Therefore, BBPSO is more suitable for the engineering application.

3. Improved MUSIC Based on NBPSO

3.1. Niche BBPSO (NBPSO). Actually, the spectrum peak search of MUSIC is a multimodal optimization problem. One of feasible methods for this problem is designing a multimodal algorithm to find all global optima and local optima as many as possible. Both the standard PSO and BBPSO are global optimization algorithms. However, they can only find out one optimal solution. In their evolution process, because of the selective pressure, they cannot get more than one global optimal solution or some better local optimal solutions. Therefore, for solving the multimodal optimization problem, scholars have introduced the niche technology into the evolutionary algorithm and presented many niche strategies, such as the preselection technique, the crowding strategy, the fitness sharing strategy, and the species conserving strategy [28].

According to the characteristics of BRB fault signal, an improved seed selection strategy is proposed in this section based on [29]. Meanwhile, we introduce it into BBPSO to form a new algorithm (named, niche bare-bones particle swarm optimization, NBPSO), which can realize the multimodal search. Comparing to [29], three differences in NBPSO are introduced: (1) the seeds are selected from the personal best positions of all particles to prevent oscillation; (2) define the species similarity σ to maintain the diversity of seeds, where σ is the Euclidean distance between any two seeds; (3) the formation of subpopulations is not dependent on the niche radius. Instead, the nonseed particles are attributed to the nearest seed. The pseudocode of improved seed selection strategy is shown in Algorithm 1 . Algorithm 1 is reproduced from the published article titled "Adaptively Choosing Neighbourhood Bests Using Species in a Particle Swarm Optimizer for Multimodal Function Optimization," which is cited in the references [28].

The seed selection strategy in Algorithm 1 is executed in each generation of evolutionary process. First, arrange all the personal best positions in the descending order with the fitness values to form a set $\boldsymbol{S}_{\boldsymbol{pbest}}$. Second, calculate the

Input: S_{pbest}-containing all particles sorted in decreasing order fitness
Output: X_s-containing dominating particles identified as species seeds

```
begin
  X_s = ∅;
  while (not reaching the end of S_pbest) do
    found ⟵ FALSE;
    for all x* ∈ X_s do
      if (d(x*, x) ≤ σ*) then
        found ⟵ TRUE;
        break;
      end (if)
    end (for)
    if (not found) then
      let X_s ⟵ X_s ∪ {x};
    end (if)
  end (while)
end
```

Algorithm 1: The algorithm for determining the species seeds.

Euclidean distances between each individual in $\boldsymbol{S_{pbest}}$ and element in the seed set $\boldsymbol{X_s}$. If all Euclidean distances are larger than σ^*, the current personal best position is added to $\boldsymbol{X_s}$.

The specific steps of NBPSO are described as follows.

Step 1. Initialize the positions of all particles, personal best positions and seed set $\boldsymbol{X_s}$. Set algorithm parameters including the population size, maximum iteration, and species similarity threshold σ^*.

Step 2. Calculate particles' fitness.

Step 3. Update particles' personal best positions $\boldsymbol{p}_i$.

Step 4. Arrange all $\boldsymbol{p}_i$ in the descending order according to the fitness values.

Step 5. Determine and update the seeds according to Algorithm 1 .

Step 6. Calculate the distance between each particle and each seed to determine which seed the particle belongs to.

Step 7. Update the positions of particles according to (11), where $\boldsymbol{p}_g$ is replaced with a seed.

Step 8. If the stop condition (the fitness error is less than the threshold or the iteration number is more than the maximum number) is met, stop the iterative procedure and output all the global optimal positions, some better local optimal positions and their fitness values. Otherwise, return to Step 2 and continue the search.

3.2. Improved MUSIC. In this section, we replace the fixed-step traversal with NBPSO in MUISC to improve the accuracy and speed of peak search. According to the characters of MUSIC spectrum, the fitness function is defined as

$$Fitness\left(x_i\right) = \left|\boldsymbol{e}\left(x_i\right)^T \cdot \boldsymbol{U_N} \cdot \boldsymbol{U_N^T} \cdot \boldsymbol{e}\left(x_i\right)\right|. \tag{12}$$

The specific steps of improved MUSIC are described as follows:

Step 1. Take a group of observation data and estimate the autocorrelation matrix $\boldsymbol{R_{yy}}$.

Step 2. Perform the eigenvalue decomposition of $\boldsymbol{R_{yy}}$ to generate the signal subspace $\boldsymbol{U}_S$ and the noise subspace $\boldsymbol{U}_N$.

Step 3. Encode f_i in (2) with real numbers and choose (12) as the fitness function.

Step 4. Search multispectral peaks using NBPSO to obtain the frequency of each component in signal $\boldsymbol{y}(n)$.

4. Least-Squares Amplitude Estimation and New BRB Fault Detection Method

4.1. Amplitude Estimation Using Least-Squares Criterion. Under the condition of BRB fault, there are three major harmonics, the fundamental harmonic and the strongest

fault-related components, around 50 Hz. So the stator current signal filtered by a band-pass filter can be represented as

$$\begin{aligned} i_m(t) = {} & \alpha_1 e^{j2\pi f_1 t} + \alpha_2 e^{-j2\pi f_1 t} + \alpha_3 e^{j2\pi f_{1-2s} t} \\ & + \alpha_4 e^{-j2\pi f_{1-2s} t} + \alpha_5 e^{j2\pi f_{1+2s} t} + \alpha_6 e^{-j2\pi f_{1+2s} t}, \end{aligned} \tag{13}$$

where f_{1-2s} and f_{1+2s} are the frequencies of the strongest fault-related components and $\boldsymbol{\alpha} = [\alpha_1, \alpha_2, \ldots, \alpha_6]^T$ is the model parameter. Since the frequency of each component in stator current can be determined accurately with the NBPSO-based MUSIC, f_1, f_{1-2s} and f_{1+2s} are considered to be known parameters. Based on least-squares criterion, define an error function $f(\boldsymbol{\alpha})$ between model current i_m and actual current i_s. To make the i_m fit the i_s, the error function value is required minimum, i.e.,

$$\min\{f(\boldsymbol{\alpha})\} = \min\left\{\sum_{i=1}^{N} r_i^2\right\}, \tag{14}$$

where $r_i = i_s(t_i) - i_m(t_i)$, $t_i = i \cdot T_s$, T_s and N are sampling interval and points.

If the error function $f(\boldsymbol{\alpha})$ reaches to a minimum, the amplitude and phase of each component in i_s can be estimated from its solution $\boldsymbol{\alpha}^*$. Therefore, how to find the least-squares solution $\boldsymbol{\alpha}^*$ is the first mission. Fortunately, (14) is a linear least-squares problem, because f_1, f_{1-2s} and f_{1+2s} can be predetermined.

Many methods have been proposed for the linear least-squares problem, such as the SVD method and the QR decomposition. For the stability and reliability, the SVD method has been widely used. This section also adopts it.

The parameters of fundamental harmonic and BRB fault-related components are estimated by the least-squares method as follows.

(1) According to the results from improved MUSIC, construct the design matrix $\boldsymbol{H}$ as follows:

$$\boldsymbol{H} = \begin{bmatrix} e^{j2\pi f_1 t_1} & e^{-j2\pi f_1 t_1} & e^{j2\pi f_{1-2s} t_1} & \cdots & e^{-j2\pi f_{1+2s} t_1} \\ e^{j2\pi f_1 t_2} & e^{-j2\pi f_1 t_2} & e^{j2\pi f_{1-2s} t_2} & \cdots & e^{-j2\pi f_{1+2s} t_2} \\ \vdots & \vdots & \vdots & \cdots & \vdots \\ e^{j2\pi f_1 t_N} & e^{-j2\pi f_1 t_N} & e^{j2\pi f_{1-2s} t_N} & \cdots & e^{-j2\pi f_{1+2s} t_N} \end{bmatrix}. \tag{15}$$

(2) Decompose $\boldsymbol{H}$ using SVD to make $\boldsymbol{H} = \boldsymbol{U}\boldsymbol{\Sigma}\boldsymbol{V}^T$, here $\boldsymbol{U}$ and $\boldsymbol{V}$ are both orthogonal matrixes, and $\boldsymbol{\Sigma} = \mathrm{diag}(\sigma_1, \sigma_2, \ldots, \sigma_6)$.

(3) Calculate $\boldsymbol{\alpha}^* = \boldsymbol{V} \cdot \boldsymbol{\Sigma}^{-1} \cdot \boldsymbol{U}^T \cdot i_s$.

(4) Estimate the amplitude and phase of each component in i_s, by calculating the modulus and argument of $\boldsymbol{\alpha}^*$.

4.2. Process of the Proposed Detection Method. Combining improved MUSIC and least-squares amplitude estimation, a new BRB fault detection method of the induction motor is proposed. As shown in Figure 1, the proposed scheme consists of four modules: Improved MUSIC, Current model, Least-square estimator, and Fault identification. In the Improved MUSIC module, the frequencies of fundamental and fault-related components are determined. Using the frequency values, the model current i_m is built. The amplitude estimate is calculated by least-square estimator. In last module, frequencies and amplitudes are used to identify BRB fault.

The specific steps of the new fault detection method are described as follows:

Step 1. Sample the stator current of one phase and estimate the autocorrelation matrix $\boldsymbol{R}_{yy}$ using current data.

Step 2. Perform the eigenvalue decomposition of $\boldsymbol{R}_{yy}$ to generate the signal subspace $\boldsymbol{S}$ and the noise subspace $\boldsymbol{G}$.

Step 3. Carry out multispectral peaks search in frequency domain by NBPSO to determine the frequency of each component in current signal.

Step 4. Corresponding to each frequency from Step 3, build the current model.

Step 5. Estimate the amplitude of each component accurately using least-squares estimation method.

Step 6. Based on the amplitude ratio of the sideband components and fundamental harmonic, it is determined whether the BRB fault occurs or not.

5. Results and Discussion Based on the Simulation and Experiment

5.1. Simulation Results and Discussion. To test the performance of the new detection method, a simulated current is built as follows.

$$\begin{aligned} i_{br}(t) = {} & I_1 \cos\left[2\pi f_1 t + \varphi_1\right] \\ & + I_{bp1} \cos\left[2\pi (1-2s) f_1 t + \varphi_{bp1}\right] \\ & + I_{bn1} \cos\left[2\pi (1+2s) f_1 t + \varphi_{bn1}\right] + n(t) \end{aligned} \tag{16}$$

where I_1=10, f_1=50, φ_1=π/3 are the parameters of fundamental harmonic. When the BRB fault is slight, the amplitudes of components at f_{br1} are much smaller than the fundamental harmonic's, and their frequency intervals are also small. Therefore, set I_{bp1}=I_{bn1}=0.2, (1-2s)f_1=49.5438, (1+2s)f_1=50.4562, φ_{bp1}=2π/3 and φ_{bn1}=8π/9. Meanwhile, $n(t)$ is a random noise with uniform distribution in the interval [-0.01, 0.01]. The sampling frequency of the simulated signal is 250Hz; the size of the data window is 500. The NBPSO parameter settings are shown in Table 1. To compare the performance, DFT and traditional MUSIC, which have been widely applied in BRB fault detection, are also performed in this simulated signal.

Data processing results of three methods are shown in Figure 2. The DFT result is not satisfactory. As Figure 2(a) shows, there is only one peak that is the fundamental harmonic. The fault-related components ((1±2s)f_1) which are

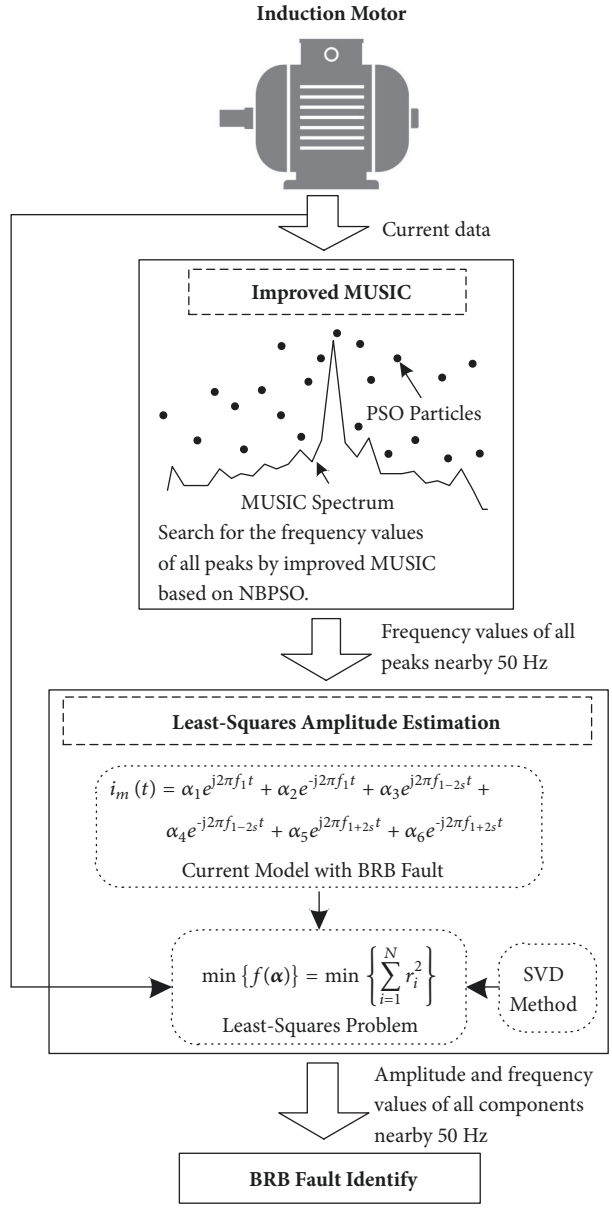

Figure 1: Block diagram of the proposed method.

Table 1: Parameter configurations of NBPSO.

Algorithm	Population size	Maximum iteration	Other parameters
NBPSO	60	30	Seed number sn=3, species similarity threshold $\sigma^* = 0.4$.

submerged completely by the fundamental harmonic are not distinguished. The reason for this case is that the frequency resolution with 2s data window is 0.5Hz, while the frequency interval between $(1\pm2s)f_1$ components and f_1 component is only 0.4562Hz. Therefore, the detection reliability of BRB fault using DFT method is low, when the data window is short. Fortunately, DFT method has very high accuracy of fundamental frequency as well as traditional MUSIC. The reason is that 50Hz is an integer multiple of the frequency resolution.

For the traditional MUSIC method, it has a very high frequency resolution, even with a short-time data window. As Figures 2(b), 2(c), and 2(d) show, the fault-related peaks are identified clearly. Due to high frequency resolution MUSIC can use shorter data window to achieve the desired frequency resolution, avoiding the impact of load fluctuations or noise in fault detection effectively. This advantage makes MUSIC suitable for the spectrum analysis of the stator current signal, especially in the BRB fault detection for the induction motor. However, the traditional MUSIC requires

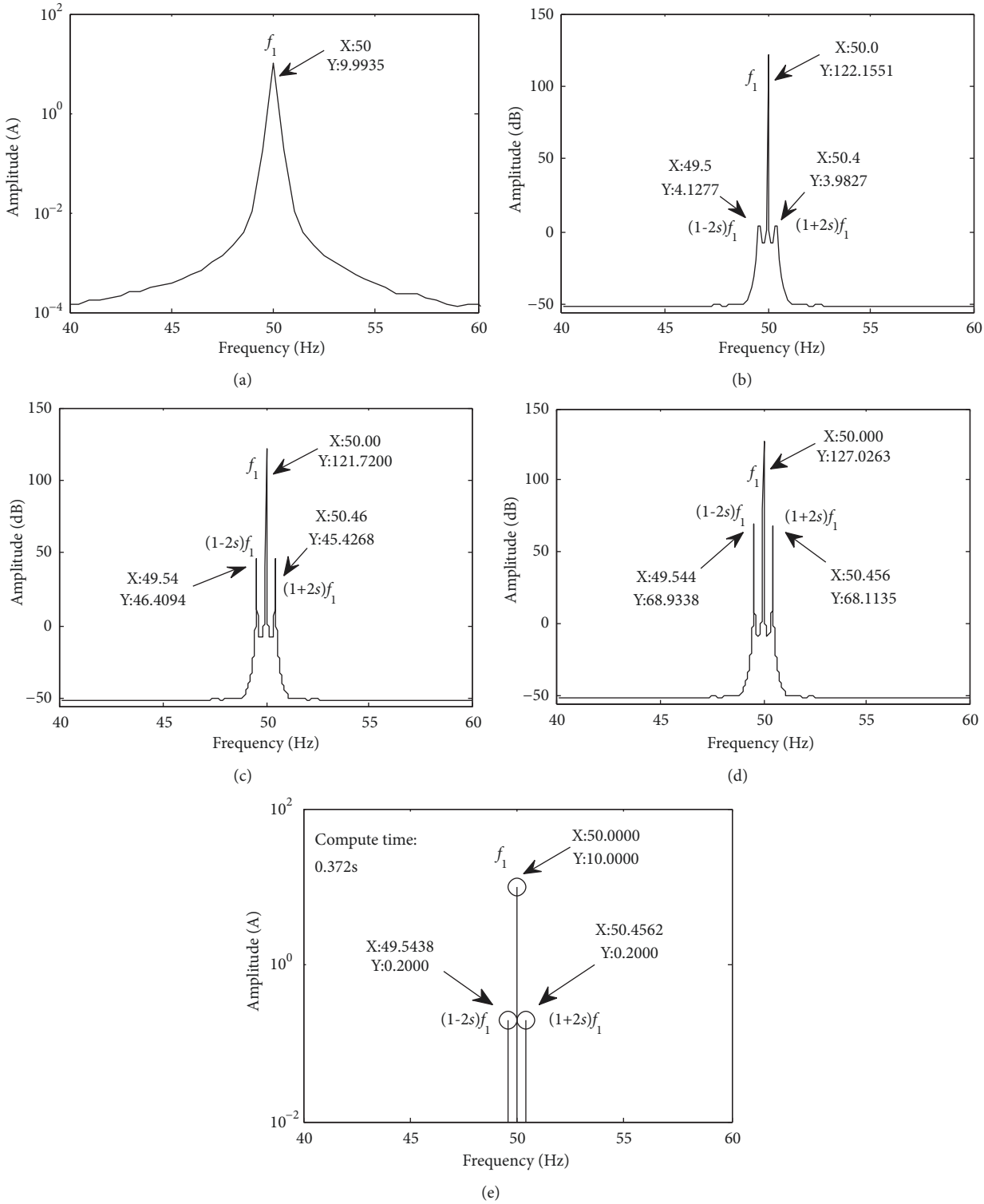

FIGURE 2: Simulated current spectrum analyzed by three methods. (a) DFT spectrum, (b) MUSIC spectrum with search step Δf=0.1 Hz, (c) MUSIC spectrum with search step Δf=0.01 Hz, (d) MUSIC spectrum with search step Δf=0.001 Hz, (e) spectrum of the proposed method.

a predetermined peak search step Δf and then traverses the whole frequency domain to find spectrum peaks. As a result of fixed-step search, the frequencies of all spectrum peaks are integer multiples of the step size. Thus frequency precision is limited. With the increase of the step size, the frequency error increases, and the peak amplitudes reduce in the spectrum. It means that the reliability of BRB detection is also limited by peak search step Δf; that is, too large search

Table 2: Statistical results of the proposed method.

Signal parameters	Actual values	Estimation result (average)	Average error	Maximum error
f_1/Hz	50.0000	50.0000	1.48×10^{-7}	3.78×10^{-5}
I_1 /A	10	10.0000	5.47×10^{-6}	8.33×10^{-5}
φ_1 /rad	$\pi/3$	1.0472	3.67×10^{-7}	2.61×10^{-4}
$(1\text{-}2s)f_1$/Hz	49.5438	49.5438	5.36×10^{-5}	7.40×10^{-4}
I_{bp1}/A	0.2	0.2000	5.00×10^{-6}	2.89×10^{-4}
φ_{bp1}/rad	$2\pi/3$	2.0941	3.41×10^{-4}	7.98×10^{-3}
$(1+2s)f_1$/Hz	50.4562	50.4562	2.81×10^{-5}	7.87×10^{-4}
I_{bn1}/A	0.2	0.2000	9.72×10^{-6}	1.53×10^{-4}
φ_{bn1}/rad	$8\pi/9$	2.7923	1.93×10^{-4}	7.52×10^{-3}

step makes the spectrum unable to identify some tiny fault-related components. Moreover, it is clear that the amplitudes of spectrum peaks obtained by MUSIC make no sense in identification of each component, even not reflecting the real magnitude value of each component.

Figure 2(e) shows the result of the proposed method. As can be seen from the graph, compared with the traditional MUSIC (search step Δf=0.001 Hz), the improved MUSIC provides a higher frequency resolution. Meanwhile, the proposed method allows it to precisely estimate the amplitudes and phases of components, while traditional MUSIC cannot. Therefore, the proposed method combining MUSIC, NBPSO, and least-squares estimation is more reliable in the BRB fault detection of the induction motor.

Since NBPSO is a stochastic optimization algorithm, it is often necessary that the proposed method is executed 50 times independently to test its robustness. The statistical results are shown in Table 2.

Comparing Figures 2(b), 2(c), and 2(d) with Table 2, it can be seen that the spectrum peak search using NBPSO improves frequency accuracy greatly. In the statistical results, the maximum frequency error is only 7.87×10^{-4} even 3.78×10^{-5} for fundamental frequency, which is more accurate than the fixed-step search of the traditional MUSIC with a step size of 0.001Hz. The average frequency error which can better reflect the accuracy of the proposed method reaches 5.36×10^{-5} (maximum of three frequency errors). By contrast, the fixed-step search requires a step size of 0.00001 Hz to achieve the same accuracy. Therefore, the improved MUSIC based on NBPSO has higher search efficiency and accuracy. It is more suitable for the BRB fault detection of the induction motor. Compared with traditional MUSIC, another advantage is that the proposed method can accurately estimate the amplitudes and initial phases of the fundamental and fault-related components. As Table 2 shows, the estimation accuracy of amplitudes reaches 9.72×10^{-6} or higher, the phases' reaches 3.41×10^{-4} or higher. In addition, to verify this method robustness, we also randomly changed the fundamental frequency, slip, and amplitude of each component in (16). The calculation accuracy of final results is consistent with Table 2.

Table 3 compares the three algorithms' computational costs. DFT has absolute advantage in this comparison; however, its frequency resolution is low with short data window. For the MUSIC, the search time increases sharply with the decrease of step. Namely, the improvement of accuracy is at the expense of computation. In contrast, the calculation cost of the proposed method is only 0.365s, which is equivalent to the traditional MUSIC in the step Δf=0.1 Hz.

Therefore, the proposed method obtains a prominent improvement on solution accuracy and search efficiency contrasting with traditional MUSIC.

5.2. Experimental Results and Discussion. The main parameters of the experimental induction motor (MODEL Y132M-4) are shown in Table 4. The experiments are carried out respectively under the conditions of half load with 1 broken bar (s=0.022) and full load with 1 broken bar (s=0.04133). The sampling interval of current signal is 7ms, and data length is 200. The waveforms of stator current signal of phase A in the two states are shown in Figure 3. The NBPSO parameters are the same as that in Table 1.

Figure 4 shows the results analyzed by MUSIC, DFT, and the proposed algorithm, respectively, on the condition of full load. In this condition, fault feature frequencies are far from the fundamental frequency, and the amplitudes of fault feature components are maximal at full load. It means that fault features are easy to be found. Thus we can see that the three algorithms can distinguish the fault feature components. However, the fault-related peaks are clearer in current spectrums analyzed by traditional MUSIC and the proposed method. The reason is that they can overcome the spectrum leakage problem well. In addition, the algorithms based on MUSIC have better frequency resolution and calculation accuracy. Figure 4 also shows that whether for fundamental frequency or for fault feature frequencies, DFT has a larger error, but it has an absolute advantage in the computational time.

Comparing Figure 4(a) with Figure 4(b), we can see that two methods all have a high accuracy in estimating the frequency of fault feature components. However, due to fixed-step search (step Δf=0.001), the frequencies estimated

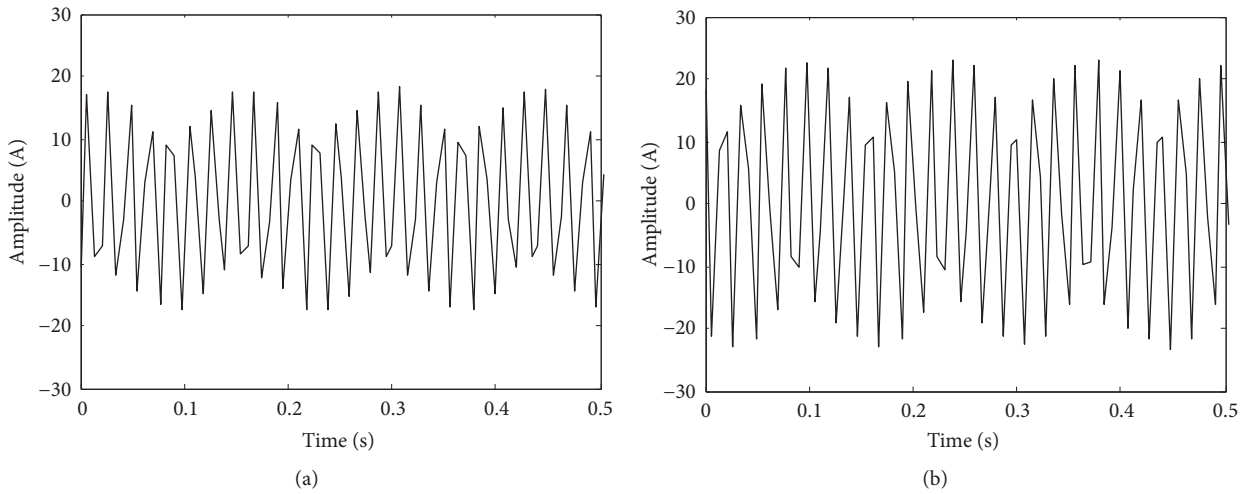

Figure 3: Waveform of stator current. (a) Full load with 1 broken bar. (b) Half load with 1 broken bar.

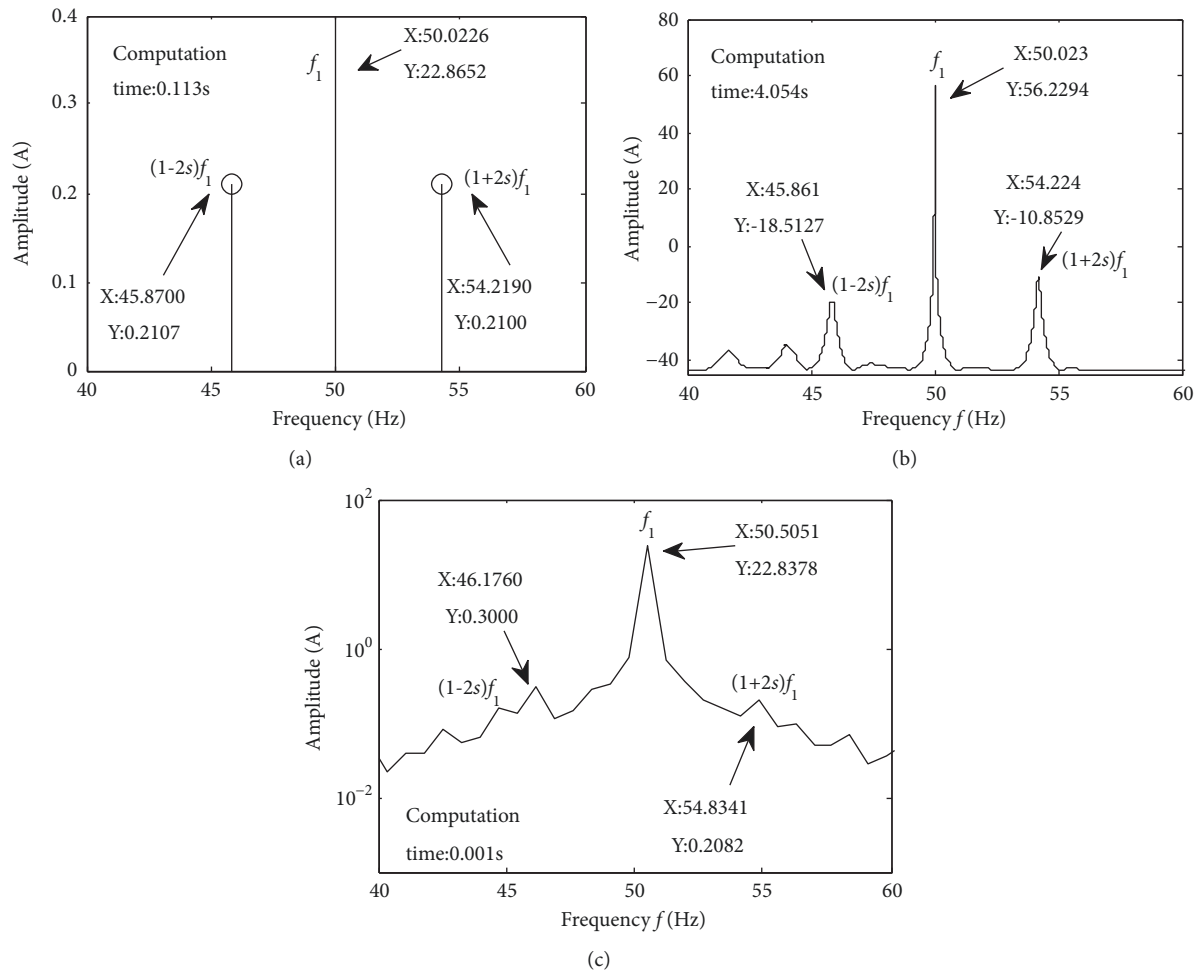

Figure 4: Spectrum of stator current under the full load. (a) Spectrum of the proposed method. (b) MUSIC spectrum. (c) DFT spectrum.

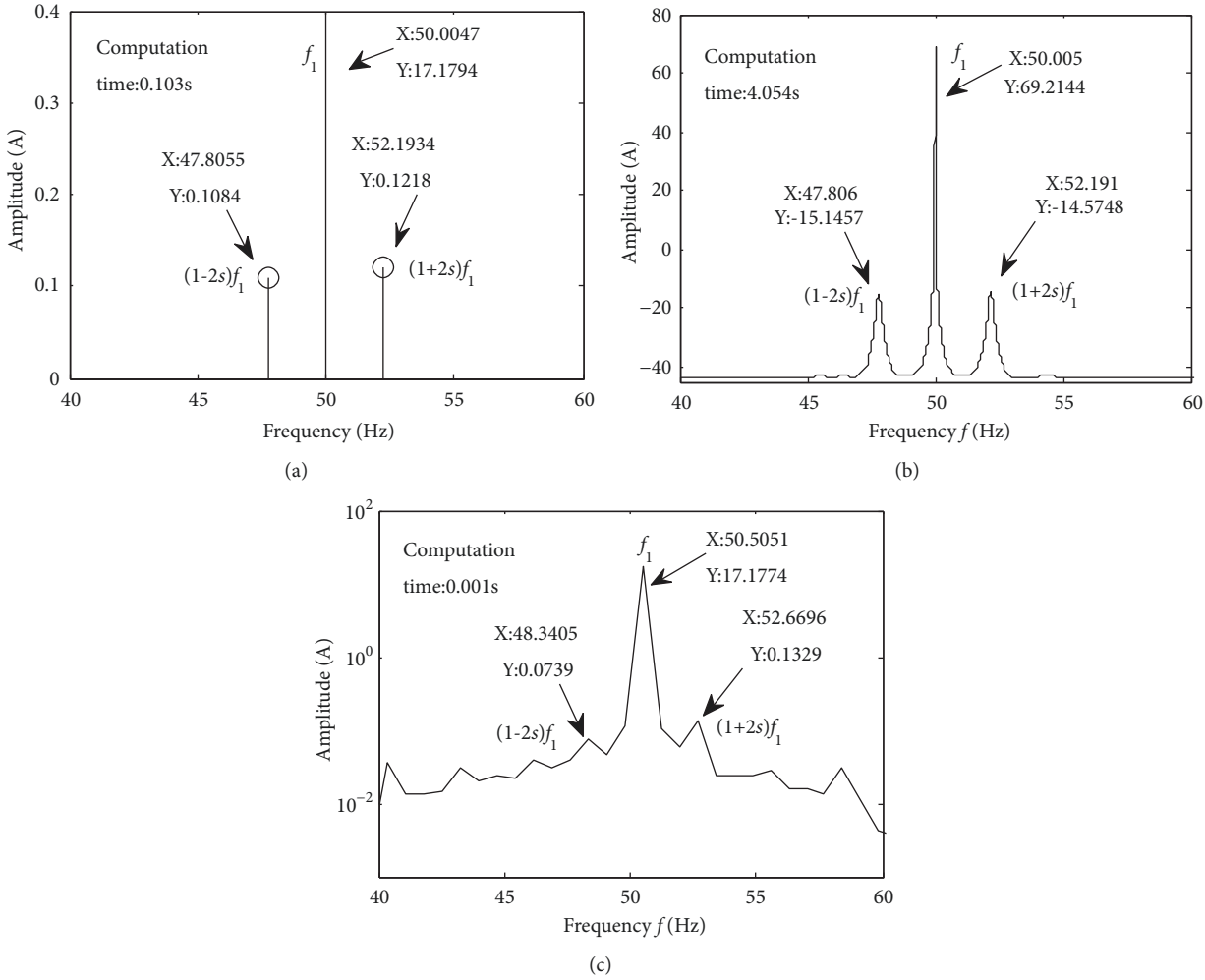

Figure 5: Spectrum of stator current under the half load. (a) Spectrum of the proposed method. (b) MUSIC spectrum. (c) DFT spectrum.

with traditional MUSIC are only the integer multiples of Δf. Therefore, the estimation results of three spectrum peaks are 45.861Hz, 50.023Hz, and 54.224Hz in Figure 4(b). Comparing Figure 4(b) and Table 5, whether for the fundamental harmonic or for the fault-related components, the proposed method can find higher spectrum peaks (with the same signal subspace and noise subspace). This cannot only prove that the spectrum peaks found by traditional MUSIC are not the true spectrum peaks, but also verify that the improved MUSIC has a higher accuracy. Moreover, the proposed method can accurately determine the amplitude and initial phase of each component signal. In addition, it also has a higher computing speed. In this experiment, its computing time is only 0.113s while traditional MUSIC's is 4.054s ($\Delta f = 0.001$).

Figure 5 shows the analysis results of the motor stator current under the half load with 1 broken bar. In this case, fault feature components are weaker and closer to fundamental harmonic in spectrum, so it is difficult to be extracted and highlighted. The characters of each method are consistent with the above analysis under the full load. Figure 5 also verifies the effectiveness, feasibility, and superiority of the proposed method.

6. Conclusions

To improve the accuracy and reliability of the BRB fault detection for induction motor, combining NBPSO-based MUSIC and least-squares amplitude estimation, a new BRB fault detection method is proposed and applied in a real motor. Although the computation cost of the proposed method is more than the DFT's, it is more reliable to detect BRB fault due to higher frequency resolution with short-time data window. Comparing with the traditional MUSIC, the proposed algorithm also has a higher accuracy, efficiency, and reliability. In our experiment of a real induction motor, two load conditions are used to verify the proposed method. The results show that it cannot only estimate the amplitude of each component accurately and improve the accuracy of spectrum peak search, but also reduce the computation time

Table 3: Computation cost comparison for the methods.

Methods	DFT	MUSIC with different search step			Proposed method (average time in 50 runs)
		Δf=0.1	Δf=0.01	Δf=0.001	
Computational cost t/s	0.001	0.101	0.814	7.732	0.365

Table 4: Specifications of the test motor.

Related power/kW	Related voltage/V	Related current/A	Related speed/ (r/min)	No. of rotor bars
7.5	380	15.4	1440	32

Table 5: Results of improved MUSIC.

Test condition	Parameters	Amplitudes of peaks/dB	Frequencies of peaks /Hz
Full load with 1 broken bar	f_1	56.7599	50.0226
	(1-2s)f_1	-18.4726	45.8700
	(1+2s)f_1	-10.8207	54.2190
Half load with 1 broken bar	f_1	70.5717	50.0047
	(1-2s)f_1	-15.1455	47.8055
	(1+2s)f_1	-14.5698	52.1934

greatly. These advantages make it more usable for fault motor operating with small slip and fluctuant load.

Data Availability

The data used to support the findings of this study are available from the corresponding author upon request.

Conflicts of Interest

The authors declare no conflicts of interest.

Acknowledgments

This work was supported by Postgraduate Research & Practice Program of Education & Teaching Reform of CUMT, National Natural Science Foundation of China (Grant No. 61703404) and Postdoctoral Science Foundation of China (Grant No. 2016M591956).

References

[1] M. O. Mustafa, G. Nikolakopoulos, and T. Gustafsson, "Broken bars fault diagnosis based on uncertainty bounds violation for three-phase induction motors," *International Transactions on Electrical Energy Systems*, vol. 25, no. 2, pp. 304–325, 2015.

[2] A. Bellini, F. Filippetti, C. Tassoni, and G.-A. Capolino, "Advances in diagnostic techniques for induction machines," *IEEE Transactions on Industrial Electronics*, vol. 55, no. 12, pp. 4109–4126, 2008.

[3] P. Shi, Z. Chen, Y. Vagapov, and Z. Zouaoui, "A new diagnosis of broken rotor bar fault extent in three phase squirrel cage induction motor," *Mechanical Systems and Signal Processing*, vol. 42, no. 1-2, pp. 388–403, 2014.

[4] S. M. A. Cruz, A. J. Marques Cardoso, "Rotor Cage Fault Diagnosis in Three-Phase Induction Motors by Extended Park's Vector Approach," *Electric Machines & Power Systems*, vol. 28, no. 4, pp. 289–299, 2000.

[5] V. F. Pires, M. Kadivonga, J. F. Martins, and A. J. Pires, "Motor square current signature analysis for induction motor rotor diagnosis," *Measurement*, vol. 46, no. 2, pp. 942–948, 2013.

[6] R. Puche-Panadero, M. Pineda-Sanchez, M. Riera-Guasp, J. Roger-Folch, E. Hurtado-Perez, and J. Perez-Cruz, "Improved resolution of the MCSA method via Hilbert transform, enabling the diagnosis of rotor asymmetries at very low slip," *IEEE Transactions on Energy Conversion*, vol. 24, no. 1, pp. 52–59, 2009.

[7] C. H. De Angelo, G. R. Bossio, and G. O. García, "Discriminating broken rotor bar from oscillating load effects using the instantaneous active and reactive powers," *IET Electric Power Applications*, vol. 4, no. 4, pp. 281–290, 2010.

[8] J. Huang, F. L. Niu, and J. Q. Yang, "Rotor fault diagnosis for induction motors based on the double PQ transformation," in *Proceedings of the CSEE*, vol. 26, pp. 135–140, 2006.

[9] P. P. Wang, L. P. Shi, Y. Zhang, and L. Han, "Broken rotor bar fault diagnosis of induction motors using a hybrid bare-bones particle swarm optimization algorithm," in *Proceedings of the CSEE*, vol. 32, pp. 73–81m, 2012.

[10] K. N. Gyftakis, A. J. Marques Cardoso, and J. A. Antonino-Daviu, "Introducing the Filtered Park's and Filtered Extended Park's Vector Approach to detect broken rotor bars in induction motors independently from the rotor slots number," *Mechanical Systems and Signal Processing*, vol. 93, pp. 30–50, 2017.

[11] D. F. Pires, V. F. Pires, J. F. Martins, and A. J. Pires, "Rotor cage fault diagnosis in three-phase induction motors based on a current and virtual flux approach," *Energy Conversion and Management*, vol. 50, no. 4, pp. 1026–1032, 2009.

[12] M. Drif and A. J. M. Cardoso, "The use of the instantaneous-reactive-power signature analysis for rotor-cage-fault diagnostics in three-phase induction motors," *IEEE Transactions on Industrial Electronics*, vol. 56, no. 11, pp. 4606–4614, 2009.

[13] C. T. Kowalski and W. Kanior, "Effectiveness of the frequency analysis of the stator current in the rotor fault detection of induction motors," in *Proceedings of the 2008 IEEE International*

Conference on Industrial Technology, IEEE ICIT 2008, China, April 2008.

[14] A. Naha, A. K. Samanta, A. Routray, and A. K. Deb, "Low Complexity Motor Current Signature Analysis Using Sub-Nyquist Strategy with Reduced Data Length," *IEEE Transactions on Instrumentation and Measurement*, vol. 66, no. 12, pp. 3249–3259, 2017.

[15] A. Sapena-Baño, M. Pineda-Sanchez, R. Puche-Panadero, J. Martinez-Roman, and Ž. Kanović, "Low-Cost Diagnosis of Rotor Asymmetries in Induction Machines Working at a Very Low Slip Using the Reduced Envelope of the Stator Current," *IEEE Transactions on Energy Conversion*, vol. 30, no. 4, pp. 1409–1419, 2015.

[16] A. Sapena-Bano, M. Pineda-Sanchez, R. Puche-Panadero et al., "Harmonic Order Tracking Analysis: A Novel Method for Fault Diagnosis in Induction Machines," *IEEE Transactions on Energy Conversion*, vol. 30, no. 3, pp. 833–841, 2015.

[17] M. A. Moussa, M. Boucherma, and A. Khezzar, "A detection method for induction motor bar fault using sidelobes leakage phenomenon of the sliding discrete fourier transform," *IEEE Transactions on Power Electronics*, vol. 32, no. 7, pp. 5560–5572, 2017.

[18] A. Garcia-Perez, R. D. J. Romero-Troncoso, E. Cabal-Yepez, and R. A. Osornio-Rios, "The application of high-resolution spectral analysis for identifying multiple combined faults in induction motors," *IEEE Transactions on Industrial Electronics*, vol. 58, no. 5, pp. 2002–2010, 2011.

[19] Y. W. Youn, H Yi, D. H. Hwang et al., "MUSIC-based diagnosis algorithm for identifying broken rotor bar faults in induction-motors using flux signal," *Journal of Electrical Engineering & Technology*, vol. 8, no. 8, pp. 288–294, 2013.

[20] D. Morinigo-Sotelo, R. D. J. Romero-Troncoso, P. A. Panagiotou, J. A. Antonino-Daviu, and K. N. Gyftakis, "Reliable Detection of Rotor Bars Breakage in Induction Motors via MUSIC and ZSC," *IEEE Transactions on Industry Applications*, vol. 54, no. 2, pp. 1224–1234, 2018.

[21] F. Fang, S.-Y. Yang, and X.-G. Hou, "Rotor fault feature extraction of motor faults of induction motor based on a modified music method," *Zhongguo Dianji Gongcheng Xuebao/Proceedings of the Chinese Society of Electrical Engineering*, vol. 27, no. 30, pp. 72–76, 2007.

[22] S. H. Kia, H. Henao, and G.-A. Capolino, "A high-resolution frequency estimation method for three-phase induction machine fault detection," *IEEE Transactions on Industrial Electronics*, vol. 54, no. 4, pp. 2305–2314, 2007.

[23] D. Camarena-Martinez, R. Osornio-Rios, R. J. Romero-Troncoso, and A. Garcia-Perez, "Detecting multiple combined faults in induction motors," *Journal of Applied Research and Technology*, vol. 13, no. 1, pp. 160–167, 2015.

[24] B. Q. Xu, L. L. Sun, and H. M. Li, "A detection method for broken rotor bar fault in induction motors based on multiple signal classification and pattern search algorithm," in *Proceedings of the CSEE*, vol. 32, pp. 93–99, 2012.

[25] R. O. Schmidt, "Multiple emitter location and signal parameter estimation," *IEEE Transactions on Antennas and Propagation*, vol. 34, no. 3, pp. 276–280, 1986.

[26] J. Kennedy and R. Eberhart, "Particle swarm optimization," in *Proceedings of the IEEE International Conference on Neural Networks (ICNN '95)*, vol. 4, pp. 1942–1948, Perth, Western Australia, November-December 1995.

[27] J. Kennedy, "Bare bones particle swarms," in *Proceedings of the 2003 IEEE Swarm Intelligence Symposium, SIS 2003*, pp. 80–87, USA, April 2003.

[28] X. Li, "Adaptively Choosing Neighbourhood Bests Using Species in a Particle Swarm Optimizer for Multimodal Function Optimization," in *Genetic and Evolutionary Computation – GECCO 2004*, vol. 3102 of *Lecture Notes in Computer Science*, pp. 105–116, Springer Berlin Heidelberg, Berlin, Heidelberg, 2004.

[29] J.-P. Li, M. E. Balazs, G. T. Parks, and P. J. Clarkson, "A species conserving genetic algorithm for multimodal function optimization," *Evolutionary Computation*, vol. 10, no. 3, pp. 207–234, 2002.